Macromolecular Crowding and Size Effects on Probe Microviscosity

Aron B. Goins, Hugo Sanabria, and M. Neal Waxham
Department of Neurobiology and Anatomy, University of Texas Health Science Center at Houston, Houston, Texas

ABSTRACT Development of biologically relevant crowding solutions necessitates improved understanding of how the relative size and density of mobile obstacles affect probe diffusion. Both the crowding density and relative size of each co-solute in a mixture will contribute to the measured microviscosity as assessed by altered translational mobility. Using multiphoton fluorescent correlation spectroscopy, this study addresses how excluded volume of dextran polymers from 10 to 500 kDa affect microviscosity quantified by measurements of calmodulin labeled with green fluorescent protein as the diffusing probe. Autocorrelation functions were fit using both a multiple-component model with maximum entropy method (MEMFCS) and an anomalous model. Anomalous diffusion was not detected, but fits of the data with the multiple-component model revealed separable modes of diffusion. When the dominant mode of diffusion from the MEMFCS analysis was used, we observed that increased excluded volume slows probe mobility as a simple exponential with crowder concentration. This behavior can be modeled with a single parameter, β, which depends on the dextran size composition. Two additional modes of diffusion were observed using MEMFCS and were interpreted as unique microviscosities. The fast mode corresponded to unhindered free diffusion as in buffer, whereas the slower agreed well with the bulk viscosity. At 10% crowder concentration, one finds a microviscosity approximately three times that of water, which mimics that reported for intracellular viscosity.

INTRODUCTION

How intracellular contents affect the mobility of single molecules is a key aspect of cell biology that is not yet fully understood. At a minimum, one can envision that immobile barriers, binding sites, and macromolecular crowding will impact intracellular diffusion, likely in distinct ways. Intracellular diffusion has been studied in vivo by varying the probe size to look for deviations from expected behavior, with varying results (1). The cell, however, is not well suited as a well controlled environment in which to observe the effects of crowding density and relative size on a probe's translational mobility, because the composition of the cell cannot be systematically varied. An exponential decrease in probe diffusion, similar to what is seen in crowded polymer solutions, has been seen in situ via osmotic manipulation of the cellular volume (2), but it is not currently possible to distinguish the effect of mobile obstacles from that of immobile barriers and other specific and nonspecific biochemical interactions.

Polymers are agents commonly used to mimic the effects of macromolecular crowding, and their size effects on probe mobility have been studied using a variety of biophysical techniques (3). Dextran and ficoll are two carbohydrate polymers that in a 12–13% (w/v) solution produce an effect on probe translational mobility similar to that determined in situ (1). When a probe exhibits only single translational mobility, as in the case of simple diffusion, its diffusion coefficient can be directly related to viscosity, and in these polymer solutions it corresponds to an increase in viscosity only severalfold that of water (1).

Using multiphoton fluorescence correlation spectroscopy (MP-FCS), we recently reported multiple diffusive mechanisms of fluorescent probes in dextran (multiple microviscosities experienced by the probe, analogous to multiple discrete diffusion coefficients) and proposed that the probe can be used as a reporter of nanostructuring of the environment (4). In this study, we examine to what extent the mobile obstacle size and crowding level impact diffusion and hence microviscosity. Because only the effects of co-solute size and crowding level on microviscosity are being evaluated, the probe size must be held constant. For this study, we wanted a model probe that would have biological significance and good spectroscopic properties, and we chose calmodulin labeled with enhanced green fluorescent protein (eGFP-CaM). eGFP-CaM is a chimeric molecule of ~43 kDa, or 3.3 nm R_h, composed of green fluorescent protein, eGFP (27 kDa), and calmodulin (16 kDa). The eGFP tag is a good fluorophore for two-photon excitation because triplet-state formation is not a significant factor as in one-photon excitation, and because its β-barrel structure shields it from environmental photobleaching (5). Calmodulin has a critical role as a Ca^{2+} sensor, and its flexibility allows it to bind promiscuously to a diverse assortment of targets, making it an important protein in biology (6). As we have previously shown that calmodulin plays an important role in neuronal synaptic plasticity (7), and have assessed calmodulin availability (8) and kinase binding stoichiometry (9), we have a motivation for understanding its

Submitted February 10, 2008, and accepted for publication August 7, 2008.

Address reprint requests to Neal Waxham, UTHSC at Houston, Neurobiology and Anatomy, U.T. Medical School at Houston, 6431 Fannin, Room 7.254, Houston, TX 77030. Tel.: 713-500-5621; E-mail: m.n.waxham@uth.tmc.edu.

Editor: Elliot L. Elson.

0006-3495/08/12/5362/12 $2.00

doi: 10.1529/biophysj.108.131250

diffusion in crowded solutions for future comparative purposes.

The extent to which crowder size composition can be used to modify a probe's mobility, and thus microviscosity, is largely unknown, especially in crowding mixtures containing crowders of many sizes. The total volume consists of the excluded volume and the volume in which the probe can freely diffuse. The excluded volume is a function of the crowding density of the obstacles, their sizes, and the size of the probe (10). To describe the excluded volume in mixtures of mobile obstacles, we have assumed that the density of different-sized polymers in a fixed volume is the same (11). Thus, we can consider that the weight-by-volume concentration of polymer (% w/v) is directly proportional to the excluded volume. This study differs from and extends earlier work in that we apply a multiple-component model to describe diffusion in systematically varied mixtures of dextran, and the microviscosities from individual crowder sizes at different-size mixtures is compared with the bulk viscosity at a biologically relevant crowding density.

MATERIALS AND METHODS

Use of microviscosity in Stokes-Einstein equation for complex solutions

We use a modified Stokes-Einstein (SE) equation to describe probe mobility, in which diffusion is inversely proportional to microviscosity rather than bulk solution viscosity. Bulk solution viscosity and diffusion are related by the SE equation, but deviations from SE are detected when probe viscosity and bulk viscosity do not agree, as is often the case in crowded polymer solutions. Thus, a closer look at its underlying formulation is warranted. The SE equation, $D = kT/6\pi\eta R_h$, shows that single-molecule diffusion, D, is driven by thermal energy (numerator), where k is the Boltzmann constant and T the temperature, and is hindered by friction (denominator), which depends on the bulk viscosity, η, and the probe's hydrodynamic radius (R_h). Einstein's relation between diffusion and probe mobility (the inverse of friction) is generally valid for probe diffusion in any solution, whereas the exact form of the friction in the SE equation, which comes from Stokes' law, applies to hydrodynamic shapes diffusing in a continuum. The SE equation without any modification seems to apply to probe diffusion in polymers if only the inverse relation between diffusion and viscosity is considered (12). However, deviations from the SE equation have been documented for probes in crowded dextran and other polymer solutions (3,13,14). These studies showed a departure from linearity when plotting normalized probe microviscosity (from diffusion measurements) versus normalized bulk viscosity, or when plotting both types of viscosity versus polymer concentration. The SE equation can still be applied to describe probe diffusion in polymer solutions, as long as the bulk viscosity is redefined as the microviscosity, which in general should not agree with the bulk viscosity except in the limiting cases of large probe size (13,15). Rather than maintaining the Stokes assumption of friction and making a direct substitution of microviscosity for ''macroviscosity'' in the SE equation, the entire denominator can be defined as the microviscosity. In either case, the same expression for normalized diffusion is obtained, which is proportional to the inverse of normalized microviscosity rather than to the inverse of normalized bulk viscosity. There is no other way for the SE equation to incorporate the effects of the probe's local environment on its mobility except through microviscosity, which instead of being a constant is minimally a function of probe and obstacle size, physicochemical properties, and crowding density.

Use of universal polymer phenomenology to describe crowded microviscosity

In crowded polymer solutions, a probe molecule's diffusion coefficient, D, is increasingly slowed as the polymer's concentration is increased according to

$$D/D_o = e^{-\beta C^n}, \quad (1)$$

where D_o is the diffusion coefficient in aqueous solution, C is the polymer concentration, and β and n are free parameters (3). Polymer phenomenology allows a direct connection between probe diffusion and environment for concentrated large mobile obstacles, although its exact connection to the mathematical theory of diffusion remains incomplete. Through use of the SE equation, Eq. 1 implies

$$\eta_\mu/\eta_o = e^{\beta C^n}, \quad (2)$$

where the normalized microviscosity for probe diffusion in polymer solutions is related to the crowding level by the parameters defined in Eq. 1. If a probe exhibits multiple diffusive behaviors, we expect that at least one can be described by Eqs. 1 and 2, although the applicability of Eqs. 1 and 2 using a multiple-component model has not been previously described.

Use of microviscosity to describe polymer size mixtures

We extend the interpretation of Eqs. 1 and 2 to describe probe mobility not only in concentrated solutions of a single polymer size but also in solutions of mixed-size polymers in which individual crowders may be dilute but all together contribute to a high overall crowding level. In a mixture of sizes, the C of Eqs. 1 and 2, rather than being the polymer concentration, is now the total polymer crowding density. The crowding density is a convenient way to describe the degree of crowding when considering dense aqueous solutions or mixtures of mobile obstacles. This can also be referred to as ''crowding level'', and is expressed as a percentage (w/v), where w is now the total polymer weight of all sizes. Crowding level is used instead of volume fraction percent (v/v), since it requires no assumptions about polymer size in terms of spatial dimensions, which are unknown and which vary in crowded solutions depending on structuring, whereas size mass (molecular weight (MW)) remains constant. The term ''size'' is used to refer to mass in the remainder of this article unless otherwise specified. The term ''concentration'' can only be used synonymously with crowding level when one size of crowder is present, whereas crowding level can be used for any type of crowding, including mixtures of multiple sizes or even multiple types of crowders. The crowding level must first be specified before probe mobility comparisons between different solutions of varying crowder size can be made.

Probe

eGFP-CaM was produced as previously described (4). Concentrated eGFP-CaM aliquots were stored at −80°C. Before each experiment, eGFP-CaM was thawed and centrifuged for 10 min at relative centrifugal force 20,800 × g and its concentration was ascertained using FCS. The stock was then diluted to make a 600-nM solution using 1× phosphate-buffered saline (PBS) lacking calcium and magnesium chloride (Invitrogen, Carlsbad, CA). The eGFP-CaM stock solution could be stored for up to several weeks at 4°C without a detectable change in its translational mobility, as ascertained by FCS.

Preparation of crowding solutions

We chose dextran as our model mobile obstacle because of its availability in a wide range of sizes and its solubility. Dextran offers the additional advantage of following the universal polymer equation (Eq. 1), which allows a connection between crowding level and microviscosity (Eq. 2). Dextran is a

carbohydrate produced by single-chain polymerization from transfer of glucosyl subunits by the enzyme dextransucrase (16). Dextran from the bacterial strain *Leuconostoc mesenteroides* NRRL B-512(F) somewhat approximates a linear polymer consisting of 95% 1,6′- and 5% 1,3′ linkages between the glucose, where branching occurring approximately every 27 subunits, with 85% of branches only one or two subunits long, though a small fraction can be much longer (16,17). Although branching only occurs to a small extent, it imparts important properties to dextran, causing it to behave as a Newtonian fluid, for example, which is atypical for a polymer, and causes bulk viscosity to have no dependence on shear rate (18). Dextran's zero-shear-rate intrinsic viscosity deviates from typical polymer behavior at high dextran MWs (17) but can be approximated with a power law $\eta \approx \mathrm{MW}^{0.47}$ for up to 500 kDa (18). At a fixed MW, dextran's viscosity at increasing concentrations follows a stretched exponential (15). As is the case for polymers in general, large deviations of the viscosity measured rheologically from that determined using microrheological techniques such as MP-FCS can occur. These deviations are more pronounced for larger-MW dextran, and the use of increasingly large probe sizes was reported to suppress the deviations (3,14).

Solutions of size-fractionated dextran from 10 to 500 kDa (10-, 40-, and 70-kDa dextran were from Amersham Biosciences, Uppsala, Sweden; 25-, 150-, 250-, and 500-kDa dextran were from Pharmacosmos A/S, Holbaek, Denmark), ranging from 5% to 30% (w/v) were made in 1× PBS. The sizes for each of the various dextran used in this study are presented in Table 1 in terms of the Stokes radius in dilute solution. The dextran used ranged from smaller to larger than the 3.3-nm-radius probe eGFP-CaM. Dextran dimensions in crowded solutions are more compact than their Stokes radii, but cannot be readily measured and vary depending on the dextran MW because of the nature of the dextran polymerization process, which results in different branching and structuring for the different sizes. The optical properties of dextran solutions >30% (w/v) prohibit accurate spectroscopic measurements in our system. Solid dextran was added to 1× PBS, mixed, sonicated briefly, and allowed to sit in a 37°C water bath until fully dissolved. The solution was then allowed to mix overnight at room temperature, and was brought to final volume using 1× PBS to make a 30% (w/v) stock solution. The solutions were stored at 4°C. The day before each experiment, a 30% dextran stock solution was diluted using first 1× PBS and then eGFP-CaM/1× PBS stock solution, for a final solution of 600 nM eGFP-CaM in 25% dextran. The process was repeated, decreasing the dextran solution in 5% increments down to 5% dextran solution, maintaining the same concentration of eGFP-CaM throughout the titration. eGFP-CaM stock solution without dextran, and the other six diluted dextran solutions (200 μL), were each placed in a separate well of an eight-chambered No. 1 coverglass slide (155411, Nalge Nunc, Rochester, NY). Microstirring bars were added to each well and the slide was then covered and mixed overnight at room temperature on a magnetic stir plate. This step was necessary to insure homogeneous distribution of the eGFP-CaM throughout the dextran solutions. On the day of the experiment, the stirring bars were removed and the slide was resealed before proceeding with spectroscopic measurements. Similarly prepared crowding solutions were made using dextrose (D-glucose), 0.18 kDa (Sigma-Aldrich, St. Louis, MO), and mixtures of the different sizes of dextran. The first dextran mixture was made with an equal mass of each size of dextran (10, 25, 40, 70, 150, 250, and 500 kDa) for crowding levels of 5–30% (w/v), and will be referred to henceforth as Dex10:500. The second dextran mixture was made with dextran of sizes equal to or larger than the probe (40, 70, 150, 250, and 500 kDa) and will be referred to as Dex40:500. Three additional mixtures of dextran, Dex10:25 (10 and 25 kDa), Dex10:40 (10, 25, and 40 kDa), and Dex70:500 (70, 150, 250, and 500 kDa), were also made at 10% (w/v). These five mixtures represent size compositions smaller than, smaller than and equal to, equal to and larger than, and larger than the size of the probe. The bulk viscosity of the five mixtures at 10% (w/v) was measured using an ARES Rheometer RDA III (Rheometric Scientific, Piscataway, NJ).

TABLE 1 Dextran size dimensions versus size mass in dilute solution

Dextran MW (kDa)	Stokes radius (nm)	Literature values (nm)
10	2.73	2.36
25	4.08	
40	5.01	4.45
70	6.39	5.8
150	8.92	
250	11.2	
500	15.1	14.7

Stokes radii were calculated using the formula of Venturoli and Rippe (11), and literature values are from a review of dextran by A. N. de Belder based on the work of Kirsti Granath (41).

Multiphoton fluorescence correlation spectroscopy

MP-FCS was accomplished as previously described (4), with 850 nm output of a Ti:Sa laser focused through a 60×, 1.2 NA water-immersion lens into a <1 fL focal volume, with measurements taken at <6 mW of power at the specimen plane. An advantage of MP-FCS is that measurements in complex fluids are readily made and all photons emitted by the fluorophore have originated from the focal volume and should contain usable information. From the fluorescence ($F(t)$) emitted by molecules diffusing in and out of the small optically-defined focal volume, the autocorrelation function $G(\tau)$ is computed in hardware via the correlator board and is mathematically represented by

$$G(\tau) = \frac{\langle \delta F(t)\delta F(t+\tau)\rangle}{\langle F(t)\rangle^2}, \tag{3}$$

which is the normalized covariance of the fluorescence signal with itself for different values of a time shift τ, where δF corresponds to deviations from the mean value $\langle F(t)\rangle$ averaged over the total time of measurement. Ten recordings over 30 s total time were obtained for each sample and averaged for further fitting. The zero time correlation represents the magnitude of the fluctuation and, for a dilute homogeneous solution, corresponds to $G(0) = 1/\langle N\rangle$. As $\langle N\rangle$ increases, fluctuations become smaller. Although $\langle N\rangle$ should be constant in this experiment, since the same concentration of probe was used in all samples, there was an apparent increase in $\langle N\rangle$ at increased crowder concentration due to increased scattered light (see Fig. S1 in Supplementary Material, Data S1, for example). For a single species chemically equilibrated in solution and diffusing in the focal volume described by a three-dimensional Gaussian function, the analytic solution for the autocorrelation function can be described as (19)

$$G(\tau) = \left(\frac{1}{N}\right)\left(\frac{1}{1+\tau/\tau_D}\right)\left(\frac{1}{1+\frac{1}{K^2}\tau/\tau_D}\right)^{1/2}. \tag{4}$$

The structure parameter of the focal volume profile is defined by K. Data were analyzed using a K of 3.2 unless otherwise specified. This value corresponds to the experimentally determined K, using a standard dye to characterize the point-spread function. The characteristic time of the diffusion, τ_D, is related to the diffusion coefficient, D, with a two-photon excitation by $\tau_D = (\omega_{xy}^2/8D)$, where ω_{xy} corresponds to the waist of the detection volume, which is specific for the objective used. For our setup, ω_{xy} is 330 nm from calibration with standard Alex546 dye in aqueous buffer, which has $D \sim 238\ \mu\mathrm{m}^2/\mathrm{s}$. Other factors have been added to Eq. 4 to describe different behaviors, such as focal volume saturation (20–22) and photobleaching (5,23,24), which are variables not considered to be necessary at the powers used in the experiments presented here, unless otherwise specified.

Objective collar correction in crowded solutions

By adjusting the collar setting on the objective, MP-FCS measurements in dextran solutions up to 30% (w/v) could be made. Manual adjustment of the

collar changes the distance between two lenses in the objective that correct for index of refraction mismatch between the immersion media and the solution as well as for the width of the coverslip, to avoid spherical aberration. The objective lens correction collar was systematically varied such that the structure parameter K was minimized, which also minimizes the effective number of molecules, N. Through experimental adjustments, the highest count rate was obtained at the optimum collar setting, yielding simultaneously the best parameters for K and N that also increased our signal/noise. Above 10% (w/v) dextran, the collar setting yielding the highest intensity was selected. Dextran of different sizes or mixtures of sizes at the same crowding level required nearly identical collar corrections, which indicates that collar setting selection has a negligible impact upon comparison of different dextran MW solutions.

Maximum entropy method fitting of a multiple-component FCS model (MEMFCS)

A multicomponent form of Eq. 4 is introduced and fit with the maximum entropy method, as previously described (4), using

$$G(\tau) = \sum_{i=1}^{n} a_i \left(\frac{1}{1+\tau/\tau_{D_i}}\right)\left(\frac{1}{1+\frac{1}{K^2}\tau/\tau_{D_i}}\right)^{1/2}, \quad (5)$$

where n, which is set at 150, is the maximum number of possible noninteracting species assumed by the model, each with a characteristic residence time τ_{Di} between 0.001 and 500 ms on a logarithmic scale. MEM (25–28) applied to FCS (29), and called MEMFCS from here on, is not only based on minimizing χ^2 to obtain an optimal fit, but also maximizes an entropic quantity $S = \sum_i p_i \ln p_i$, which is related to each of the amplitudes (a_i) by

$$p_i = \frac{a_i}{\sum_j a_j}. \quad (6)$$

MEMFCS takes the oversampled data (ten 30-s takes for each sample) and finds the least biased probability p_i of each τ_{Di} based on the data. For this multicomponent model, one has to consider that $G(0)$, instead of corresponding to the inverse of the number of molecules for one component, now corresponds to the sum of all the amplitudes ($G(0) = \sum_j a_j$). By normalizing the amplitudes, a_i, by dividing by $G(0)$, p_i from Eq. 6 now represents the probability that a species i has a translational residence time, τ_{Di}.

MEMFCS typically detects a distribution of diffusion times, τ_{Di}s, which can be very narrow, consisting of only a few τ_{Di}s each, with a high probability in the case of probe in buffer, or can broaden or distinguish discrete distributions in the case of probe in crowded dextran solutions. The point at which a distribution was maximized was called τ_{Dmax}. When more than one distribution was observed, the diffusive component possessing the τ_{Dmax}, with the highest-probability amplitude, was classified as major and diffusion mechanisms with lower-probability distributions as minor. The detection and magnitude of minor diffusive components from the MEMFCS fitting are highly sensitive to the change in slope of the correlated data. Having ruled out standard FCS artifacts, focal volume uncertainty and noisy data are the primary obstacles affecting accuracy of detection of the minor components. The shape of the focal volume in buffer can be reasonably approximated with a three-dimensional Gaussian profile (30), and the lateral dimension of the focal volume in MP-FCS should be constant even up to high levels of scattering (31). The axial/radial volume aspect ratio (K), when allowed to vary, increases from 3.2, obtained in buffer, to ~6 at 30% (w/v) crowding level of dextran when fit with the single-component model. However, we interpret this apparent change in K to be due to deviations in the data itself (such as the appearance of multiple-component or anomalous diffusion). Because there is no compelling evidence to suggest that K increases significantly with crowding, we held it constant at 3.2 for all MEMFCS data shown. An increase in K caused by spherical aberration should be negligible, because the adjustment for solution index of refraction was made using the objective collar.

Anomalous diffusion

Another possible way to describe complex diffusion in heterogeneous environments is by assuming the phenomenological description ''anomalous diffusion'', which occurs when the mean-squared displacement follows a power law in the form

$$\langle r^2(t)\rangle = 6\Gamma t^{\alpha}, \quad (7)$$

where α encompasses deviations from normal diffusion ($\alpha = 1$) and Γ is a constant that does not depend on time. However, if an apparent diffusion coefficient is defined, then Γ will depend on the timescale or, equivalently, the lengthscale of the measurement. The phenomenon for the case of $\alpha < 1$ has been termed subdiffusion, whereas the case of $\alpha > 1$ is termed superdiffusion. Including the α exponent in Eq. 4 (32) leads to

$$G(\tau) = \left(\frac{1}{N}\right)\left(\frac{1}{1+(\tau/\tau_{Da})^{\alpha}}\right)\left(\frac{1}{1+\frac{1}{K^2}(\tau/\tau_{Da})^{\alpha}}\right)^{1/2}. \quad (8)$$

The residence time is denoted now by τ_{Da} to differentiate it from τ_D. To fit the anomalous model, K was set to 3.2. K and α are not independent, and the increase of scattered light caused by increasing crowder concentration might have a slight impact on K, and thus on α. Analyses using K set to 2.5, 3.2, and 5 were used to estimate the K-dependent error. The α values increase or decrease uniformly with increase or decrease of K, indicating that relative trends in α with different crowder solutions are K-independent. We specify that $\alpha \geq 0.85$ is not anomalous, because values of 0.5–0.75 are usually considered subdiffusion (33).

RESULTS

Effect of crowding on autocorrelated data

Using multiphoton fluorescent correlation spectroscopy, this study addresses how dextran size and crowding level influence the translational diffusion of eGFP-CaM, a protein of 43 kDa (~3.3-nm R_h). For each size and size mixture of dextran, the crowding level was increased from 0 to 30% (w/v) and the detected fluorescence was autocorrelated (Eq. 3). To obtain quantitative information from this raw data and to attempt comparison with polymer diffusion phenomenology and models, an appropriate MP-FCS model must be applied. Fig. 1 shows a comparison of the three models fitting eGFP-CaM diffusion in 30% (w/v) dextran 500 (Dex 500). The slope of the decay on the correlated data is the reason the single-component model (*fcs*, $\tau_D \sim 6.85$ ms) does not fit the crowded data and appears too high to the left of the point of inflection, $G(\tau_D)$, and too low to the right, so we discard a single-component model as inappropriate to fit this data. The multiple-component model (*memfcs*) fit uses additional characteristic times of diffusion for an improved fitting ($\tau_{Dmax,minor} \sim 1.05$ ms and $\tau_{Dmax,major} \sim 7.97$ ms), and the anomalous model ($\tau_{Da} \sim 6.38$ ms) improves fitting by introduction of an additional parameter, α ($\alpha = 0.961$).

Anomalous model fitting of diffusion in crowded dextrans

The MP-FCS anomalous model (Eq. 8), an approximation to anomalous diffusion, incorporates an additional fitting parameter, α, meant to reveal nonlinearities in diffusion of

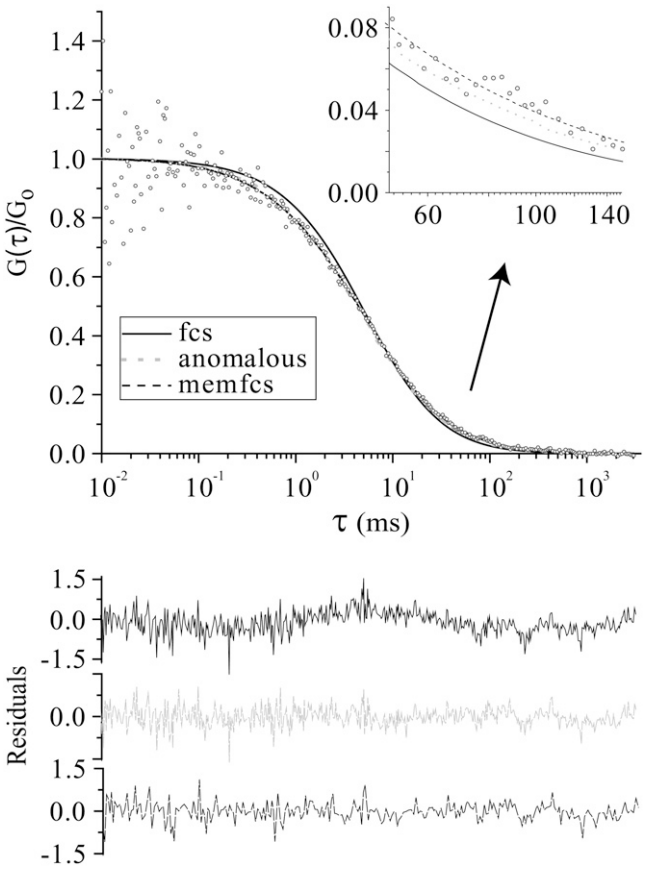

FIGURE 1 Comparison of three models for fitting autocorrelated photon counts and fitting residuals. Normalized autocorrelation (*y* axis) plotted against the time delay τ (*x* axis) for autocorrelated photon counts fit with a single-component model (*fcs*, $\tau_D \sim 6.85$ ms), anomalous model (*anomalous*, $\tau_{Da} \sim 6.38$ ms and $\alpha \sim 0.961$), and multiple-component model (*memfcs*, $\tau_{Dmax,minor} \sim 1.05$ ms and $\tau_{Dmax,major} \sim 7.97$ ms). (*Inset*) Zoomed-in region illustrating differences in fitting for this particular probe-polymer system (600 nM eGFP-CaM in 30% (w/v) Dex 500). Both the anomalous and MEMFCS models fit the data well. The single-component model (*fcs*) does not.

molecules with respect to time (Eq. 7). The α values obtained for all dextran sizes and the mixture over the concentration range studied are presented in Fig. 2. Data is fit with $K = 3.2$, but error bars are calculated using $K = 2.5$ and 5 to show that results are *K*-independent, since the shift in α with *K* is uniform. Simple diffusion is defined as having $\alpha = 1$, and given the statistical variability in the data, we considered an α value <0.85 necessary to reliably indicate anomalous diffusion. None of the data met this criterion (Fig. 2). The lowest α values were obtained for dextran 250 at 15% and 25%(w/v). As there is no direct physical interpretation for a decreased α-value, there seems little to be gained from fitting this data of 3D probe diffusion in crowded environments to an anomalous model.

MEMFCS reveals multiple microviscosities with crowding

All of the data analyzed by the anomalous model were also analyzed with a multiple-component model (Eq. 5). Traditionally, the number of components to be fit must be assigned a priori (i.e., 1, 2, 3, etc.), which may or may not be valid for the physical system being described. The use of the maximum entropy method for FCS (MEMFCS) minimizes this problem by determining the number of components required based on the statistical properties of the dataset. When MEMFCS is applied to autocorrelated data from eGFP-CaM in buffer, it agrees extremely well with the single-component model (see Fig. S2 in Data S1). Within the crowded-environment parameter space examined in this study, MEMFCS most often reveals two main distributions of diffusion times.

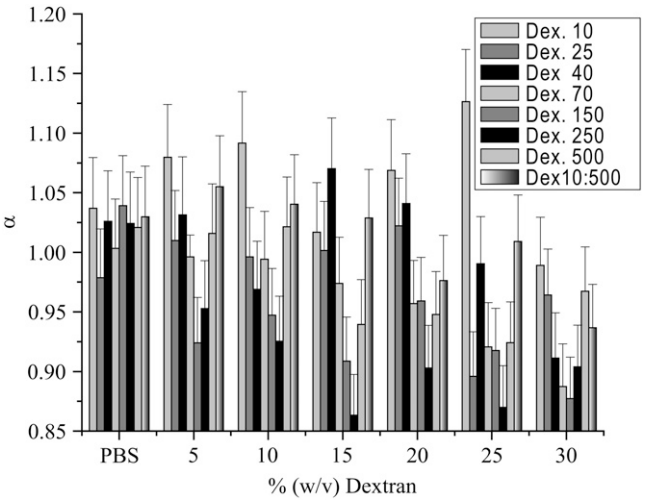

FIGURE 2 Summary graph of fits using the anomalous model for eGFP-CaM diffusion in different dextran solutions at different concentratoins. The autocorrelation data was fit with Eq. 8 and the derived α values are plotted against the concentration of each sized dextran. Note that none of the data achieves an α value <0.85, which means that none of the data meet the criteria for anomalous subdiffusion.

When multiple peaks on the τ_{Di} distribution were observed, we classified them by choosing the major diffusive component to be the one with highest probability. The minor component was classified as the lower-probability distribution. It is important to note that the major component in crowded solutions, τ_{Dmax}, mostly agrees with the single-component fit, τ_D, and with $\tau_{D\alpha}$, accounting for most of the phenomenology described therein. Each τ_{Dmax} of each distribution was then converted into a microviscosity by the modified SE relationship.

For each dextran size, crowding was increased up to 30% (w/v) and for each crowding level, a probability distribution was obtained that can reveal multiple diffusive components. MEMFCS probability distribution fittings for eGFP-CaM in Dex 500 are shown in Fig. 3 *A*. Note that the peak of the distribution is relatively sharp in 5% and 10% solutions, but starts to broaden at 15%, where a second slower diffusing component is also evident. At 20% and 25%, a similar bimodal distribution is evident. These distinct peaks are likely due to nanostructuring of the dextran solutions. There is also a systematic slowing of diffusion as the crowding level of the 500 kDa dextran solution is increased, as anticipated. By taking

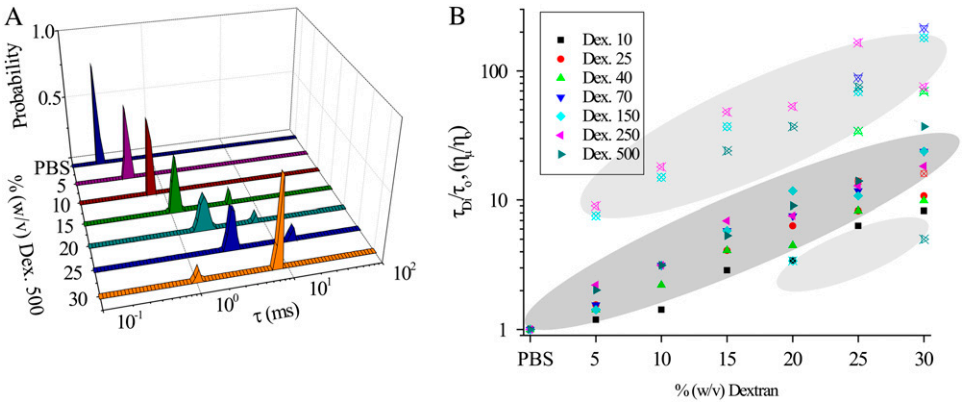

FIGURE 3 Multimodal behavior of diffusion at increasing concentrations of dextran. (*A*) MEMFCS fits of probe eGFP-CaM diffusion in crowding levels up to 30% (w/v) of Dex 500. (*B*) Summary plot of the multiple modes of normalized diffusion (τ_D/τ_o), which are also plotted as normalized microviscosities (η_μ/η_o) derived from the MEMFCS fits for each dextran size and crowding level from 5% to 30% (w/v). The solid symbols represent the major microviscosity and the open crossed symbols represent the minor microviscosity. Three regimes of normalized microviscosity were identified in the data: the major microviscosity regime is dark gray and two regions of minor microviscosity are in light gray.

the peak τ_{Di}(s) from MEMFCS probability distributions and normalizing those values to eGFP-CaM in buffer ($\tau_D = 0.21$ ms), we can relate the translational diffusion to a normalized apparent microviscosity (η_μ/η_o). This was done for the data from each dextran solution and the plot is shown in Fig. 3 *B*. We highlight in this plot the major component (largest peak from the probability distribution) in dark gray and the minor components in light gray. The fraction of probe molecules producing the minor component on average is 12.0% of the total MEMFCS probability distribution, indicating either that 12% of the probe population (~10 of 80 molecules for 600 nM probe) experiences the minor viscosity or, alternatively, that each individual probe molecule experiences the minor viscosity 12% of the time it resides in the focal volume. The remaining 88% of the probability distribution can be described by the universal polymer equation. The major (first) and minor (second) microviscosity for eGFP-CaM diffusion in glucose (the dextran monomer) in each size of dextran and in the mix of all sizes is summarized in Table 2. Probe mobility is slowed threefold at 10% (w/v) for all of the dextran sizes, except for 10 and 40 kDa, which require 15% (w/v) to achieve a threefold slowing. The frequency of apparent nanostructuring in general increases with increasing crowding level and dextran MW and, interestingly, the mixture of all dextran sizes (Dex10:500) shows suppressed nanostructuring.

Comparison of microviscosities and bulk viscosity

It is of significant interest to relate how measurements of probe diffusion (microviscosity) relate to the bulk viscosity of the polymer solutions. In Table 3, bulk viscosity determined from rheometry is shown for each dextran size and size mixture, and it can be seen that bulk viscosity increases with dextran size composition at a fixed crowding level. In Fig. 4, the bulk viscosity is plotted along with the microviscosities determined from MEMFCS fitting of the MP-FCS data. Unlike the bulk viscosity, the majority of the probe viscosity is constant for fixed crowding level, indicating that volume exclusion, rather than mobile obstacle size, dominates the probe's translational mobility. The major component of microviscosity measured using MEMFCS fitting reveals that at 10% (w/v) crowding level, eGFP-CaM's mobility is slowed approximately threefold relative to that of buffer and is independent of the solution's crowder size composition, whether it is diffusing in the presence of individual dextran sizes (Fig. 4 *B*) or in mixtures of different dextran sizes (Fig. 4 *A*).

TABLE 2 Microviscosity of eGFP-CaM in dextran

% (w/v)	Dex 10	Dex 25	Dex 40	Dex 70	Dex 150	Dex 250	Dex 500	Dex10:500
5	1.2	1.6	1.4	1.6	1.4, 7.6	2.2, 9.0	2	1.7
10	1.4	3.1	2.2, 9.0	3.1	3.2, 15	3.1, 18	3.1	2.9
15	2.9	4.1	4.1	5.8	5.8, 37	6.9, 48	5.3, 24	4.9
20	3.4	6.4	4.5	7.6	12, 3.4	7.6, 53	9.0, 37	6.4, 17
25	6.4	8.3, 14	8.3, 34	12, 89	11, 69	13, 165	14, 75	11
30	8.3	11, 16	9.9, 69	24, 215	24, 181	18, 75	37, 5.0	17, 97

Microviscosity, η_μ/η_o, for each size of dextran, from 10 to 500 kDa, and the dextran mix of all sizes for each crowding level, 5–30% (w/v). Entries with two values represent the major (first) and minor (second) components resolved by MEM-FCS fitting of the data.

TABLE 3 Bulk viscosity of dextran solutions

Viscogen 10% (w/v)	Viscosity (cP)	Standard deviation
Dex 10	2.28	0.03
Dex 25	3.40	0.04
Dex 40	4.59	0.04
Dex 70	6.23	0.05
Dex 150	14.27	0.13
Dex 250	15.82	0.14
Dex 500	18.83	0.22
Dex10:25	2.57	0.03
Dex10:40	2.81	0.03
Dex40:500	6.56	0.06
Dex70:500	8.61	0.08
Dex10:500	14.29	0.12

Bulk viscosity of each size dextran solution for each viscogen size and mixture size composition at 10% (w/v) crowding level.

The only exception is data from probe diffusing in 10-kDa dextran (Dex 10) in which the crowder size effects outweigh the crowding level effects, and an increased crowding level is required to obtain the same reduction in translational mobility. Unlike the major component of microviscosity, the bulk viscosity of dextran is highly sensitive to the co-solute size composition. Dextran's bulk viscosity at 10% (w/v) increases as a power law approximating $MW^{0.6}$ with increasing dextran size. It is interesting to note that the bulk viscosity is near the major component of microviscosity until 40 kDa, at which point a significant deviation between bulk and microviscosity is evident. For three of the co-solute sizes (40, 150, and 250 kDa), a minor component of microviscosity is detected that consists of 9–12% of the MEMFCS diffusion probability, which can be greater than or similar to the bulk viscosity (Fig. 4 *B*).

The bulk viscosity of the dextran mixtures increases with increasing crowder size composition relative to the probe (Fig. 4 *A*). The Dex10:25 and Dex10:40 mixtures have similar bulk and major microviscosities, approximately threefold that of buffer, with minor microviscosities nearly the same as that of buffer, indicating that a minor fraction of the probe—35% and 39% distribution probability, respectively—experiences a viscosity similar to that in buffer. The Dex40:500 and Dex70:500 mixtures have minor microviscosities that agree with the bulk viscosity, consisting of 17% and 9%, respectively, of the MEMFCS distribution probability (Fig. 4 *A*). These results indicate that the major component of translational diffusion is slower relative to buffer, but is independent of the size of the crowding agent whether the crowders are homogeneous (Fig. 4 *B*) or in mixtures of different sizes (Fig. 4 *A*). The results also indicate that in solutions of certain dextran sizes, a small but significant fraction of the probe diffuses in proportion to the bulk viscosity of the medium.

Application of the universal polymer equation

MEMFCS can reveal multiple microviscosities for a given dextran at a fixed crowding level, but polymer phenomenology only applies for a single microviscosity. Nonetheless, the major microviscosity detected by MEMFCS accounts for most of the phenomena observed, ~80% of the population (on average), and we use this microviscosity to describe the physical parameters of the crowded solutions. Of all the dextran sizes examined, only the 10-kDa solution shows no minor components of microviscosity with eGFP-CaM as the probe molecule. We used this data first to relate our experimental findings to the universal polymer equation (Eq. 2). Fig. 5 *A* shows the amplitude distribution of τ_{Di}s from MEMFCS fitting for concentrations ranging from 0 to 30% (w/v) Dex 10. Again, these τ_{Di} values normalized against the τ_D of the probe translational diffusion coefficient in buffer can be directly transformed to the normalized microviscosity (η_μ/η_o). Fig. 5 *B* shows the exponential behavior of the major component as a function of crowding level or excluded volume. If one uses the universal polymer equation (Eq. 2) to fit the data (first fixing

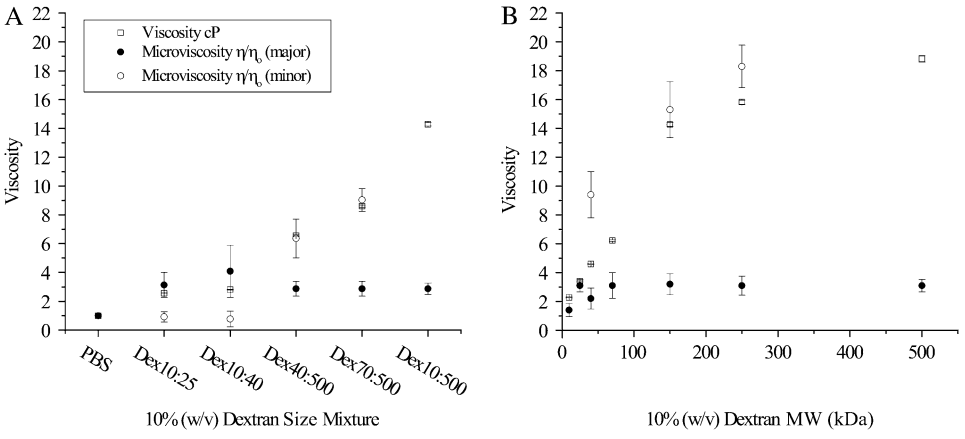

FIGURE 4 Relationship between bulk viscosity and microviscosity. Rheology measurements were used to obtain the bulk viscosity of 10% (w/v) solutions of each of the indicated dextrans, and this data is plotted along with the microviscosity of eGFP-CaM (43 kDa) diffusion determined from MEMFCS fits. (*A*) The bulk viscosity and microviscosities of various mixtures of dextran. The major peak of microviscosity increases to approximately threefold that of buffer, but then plateaus. A fraction of probe experiences a second microviscosity, which can either be freely diffusing, as in buffer (Dex10:25, 35%; Dex10:40, 39%); equal to the bulk viscosity (Dex40:500, 17%; Dex70:500, 9%); or not apparent at all (Dex10:500). (*B*) Probe viscosity in individual dextran sizes. The microviscosity (major component) increases to about threefold that in buffer, but then is relatively constant, whereas the bulk solution viscosity increases via a power law as the dextran size increases. A minor component of microviscosity (~10% of the total amplitude) is detected that can be greater than or equal to the bulk viscosity in Dex 40, 150, and 250.

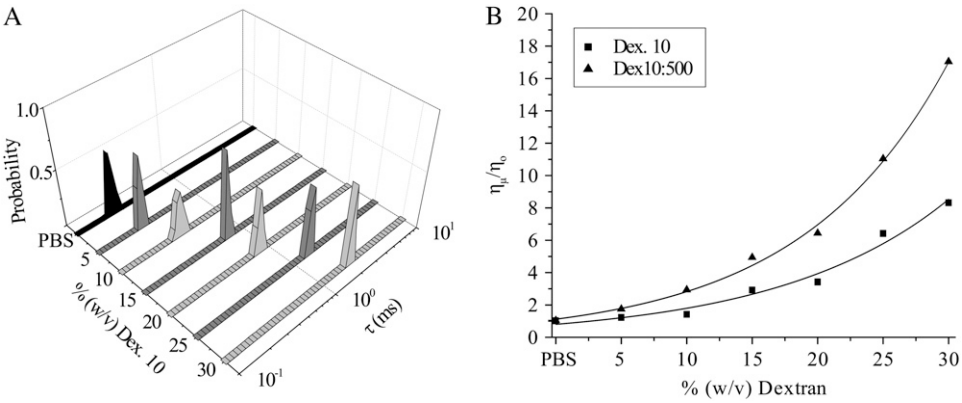

FIGURE 5 Exponential slowing of diffusion in dextran with increased concentration. (*A*) MEMFCS fits of eGFP-CaM diffusion in Dex 10 for crowding levels up to 30% (w/v). The distributions are all unimodal (agree with single-component model fits). (*B*) The normalized microviscosity (η_μ/η_o) of the Dex 10 and Dex10:500 mixtures are plotted against concentration, and fits to this data (Eq. 2) indicate that the microviscosity increases exponentially. For the mixture, minor components of microviscosity are ignored for clarity.

$n = 1$), the major component of microviscosity for the 10-kDa dextran data is best fit with a simple exponential that defines the parameter β, which is 0.076. In the Dex10:500 mixture, a similar exponential increase in relative microviscosity is seen with increasing crowding level (Fig. 5 *B*), and β in this circumstance is 0.094.

In a similar way, we determined the value of β for each dextran MW by linear regression of a semilog plot of the percent dextran versus the normalized microviscosity (Fig. 6 *A*). The line in Fig. 6 *A* actually represents the linear regression through the average of all the dextran solutions, which produced a β_{avg} of 0.098. This value for β is very close to the β-value obtained from the Dex10:500 mixture, $\beta = 0.094$. A summary graph presenting the β-values versus the MW dextran (in semilog) is shown in Fig. 6 *B*. A linear regression of this data reveals a relationship of $\beta = \mathrm{MW}^{0.11}$. Overall, β is shown to increase with the MW of dextran used for reference; the β-value of the Dex10:500 mixture is represented by the horizontal dashed line (Fig. 6 *B*). Table 4 contains the β-values for the simple-exponential fits (Eq. 2; $n = 1$), as well as the stretched exponential fits (Eq. 2; n as a free parameter) for comparison to other polymers. The β from the simple fits has an averaged low value of 0.077 for the small dextran (10, 25, and 40 kDa) and an averaged high value of 0.106 for the larger-sized dextran (70, 150, 250, and 500 kDa), with the transition occurring when the size of viscogen becomes larger than the size of the probe (43 kDa). The β from the stretched fits has no clear trend, ranging from 0.016 to 0.240, with n ranging from 0.70 to 1.135. Only data from dextran 250 is fit slightly better with a stretched exponential. Glucose, the dextran monomer, could be fit with an exponential over the concentration range tested, as expected (34), and displayed the lowest β-value, 0.027 (data not shown). The n values obtained for glucose, Dex 10, Dex 70, and Dex10:500 (the mixture of all sizes) are 1.07, 1.13, 1.10, and 1.10, in rough agreement with the simple-exponential fit, whereas the other dextran sizes have values ranging from 0.70 to 0.87.

DISCUSSION

MEMFCS model for diffusion in crowded mobile obstacles

MP-FCS is a powerful technique for studying the translational mobility of fluorescent probes in heterogeneous solutions. To what extent inert mobile obstacles alone can affect probe

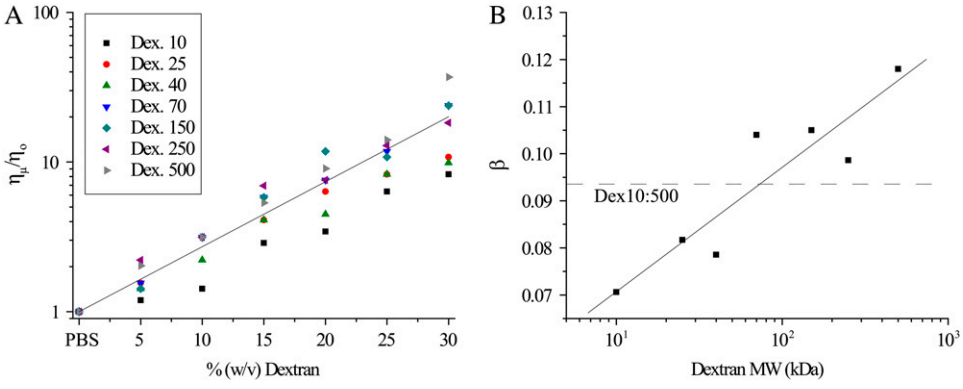

FIGURE 6 Normalized microviscosities for probe in each individual dextran size. The major component from the MEMFCS fit of probe mobility in each dextran solution was converted to normalized microviscosity (η_μ/η_o) and this was plotted against the crowding level (5–30% w/v). The line represents a linear regression through the average of all the data. The resultant parameter $\beta = 0.098$ is in close agreement with β from the Dex10:500 mixture. (*B*) The parameter β from fits to each dextran solution shown in *A* were plotted against the MW of each dextran. The line shows a linear fit with MW that on this semilog plot produces the relationship of $\beta \approx \mathrm{MW}^{0.11}$. The dashed line indicates the β-value obtained from the Dex10:500 mixture, which shows an intermediate value of 0.094.

TABLE 4 Polymer phenomenology for eGFP-CaM in dextran

Viscogen	β	n	RMSE	β (stretched)	n (stretched)	RMSE
Glucose 0.18	0.03	1	0.24	0.02	1.08	0.12
Dex 10	0.07	1	0.44	0.05	1.14	0.47
Dex 25	0.08	1	0.79	0.22	0.70	0.30
Dex 40	0.08	1	0.66	0.13	0.84	0.67
Dex 70	0.10	1	0.96	0.08	1.10	1.08
Dex 150	0.11	1	1.98	0.24	0.76	2.32
Dex 250	0.10	1	1.25	0.23	0.74	0.75
Dex 500	0.12	1	2.41	0.16	0.87	1.82
Dex10:500	0.09	1	0.37	0.08	1.11	0.33

The free parameters β and n of the universal polymer equation (Eq. 2) for simple exponential ($n = 1$) and stretched exponential fits from the major components resolved by MEM-FCS fitting of the data from eGFP-CaM diffusion in 0–30% (w/v) viscogen with root mean-squared errors (RMSE).

mobility is largely unknown, but must be established as part of a larger effort to understand protein diffusion and, thus, transport and signaling capacity in vivo. MEMFCS has been applied to such data to reveal multiple diffusive mechanisms of eGFP-CaM (43 kDa) mobility in Dex 500 and to potentially reveal multiple diffusive mechanisms of apparent nanostructuring (4), reminiscent of that seen for probe mobility in vivo. Using these techniques, we examined the effects of the crowding level and viscogen size on eGFP-CaM translational mobility and related the multiple diffusive components detected (major and minor) to the local microviscosity experienced by the probe (Table 2). This work extends the findings for eGFP-CaM translational mobility crowded with mobile obstacles to include sizes from 10 to 500 kDa, as well as mixtures of those sizes.

Anomalous diffusion (Eq. 8) has been reported in Dex 500 for some probes (33), but has not been reported for a large range of probe sizes (35), and is not seen for eGFP-CaM except in the presence of immobile obstacles (4). We observed a similar lack of evidence for anomalous diffusion in this study (Fig. 2). Instead, we found that the use of a multiple-component model of simple diffusion (Eq. 5) adequately describes eGFP-CaM mobility, in agreement with the single-component model (Eq. 4) in the limit of small viscogen size and dilute crowding level. In solutions of crowded mobile obstacles that approach and surpass the size of the probe, the single-component model ultimately fails as the appearance of bimodal or fully separated distributions of diffusion times become evident with MEMFCS fitting.

MEMFCS reveals evidence of multiple microviscosities

FCS relates diffusion time with the diffusion coefficient, and the SE equation relates the diffusion coefficient to microviscosity. Thus, the peak of each distribution revealed by MEMFCS fits can be used to calculate a discrete microviscosity. We find that for eGFP-CaM in dextran, up to three discrete microviscosities can be detected, one major and up to two minor. The amplitude of major microviscosity can be similar to that of bulk viscosity or much less, depending on viscogen size (Tables 2 and 3), but can always be described by polymer phenomenology, even for mixtures, over the entire range of crowding (Table 4). The minor microviscosity, which is not always detected, can either be less than the major microviscosity, corresponding to unhindered free diffusion, or higher than the major microviscosity, which can be similar in magnitude to bulk viscosity (Fig. 4). In a similar way, we find that multiple components are evident in crowded solutions of bovine serum albumin (data not shown), but potential binding and charge effects and autofluorescence complicate simple interpretation of probe diffusion in such protein solutions.

Major microviscosity described by polymer phenomenology

No theory yet exists that is adequate to describe the multiple diffusive mechanisms we detected in crowded solutions of dextran. However, because most (>80%) of the diffusive behavior is captured by the major microviscosity, and because it can be described by polymer phenomenology (Eqs. 1 and 2), a relation can be made at least between the major microviscosity and polymer theory. The microviscosity in the universal polymer phenomenology (Eq. 2) only has two free parameters, n and β, which are fit over a range of crowding levels, C, whose exact functional dependence is not completely agreed upon, since it depends on the polymer model assumed (36,37). Whether the parameter β is independent of MW or increases with dextran MW as a power law or in some other way remains unclear (14,15). The constant n is most likely related to solvent quality (36,38) and size of the polymer (3), whereas β is related to the size of the polymer (3) and/or the size of the probe (39,40). For most linear polymers, n is expected to be $\sim$0.75 which is supposed to indicate good solvent quality. Dextran is not a linear polymer, and both higher and lower n values, ranging from 0.53 to 1.35, have been reported for different probe mobilities in different concentrations and sizes of dextran (14,15,33,35). Dextran in this regard behaves more like a carbohydrate than a standard polymer, where values of $n > 0.75$ and even $n = 1$ are not unexpected (34). Water is considered to be a good solvent for dextran (36).

By experimentally determining the free parameters, probe microviscosity for our fixed probe size can be modeled not only in terms of the environment crowding level, but also in terms of obstacle sizes. The results of this work clearly indicate that polymer phenomenology does indeed apply to the major component of microviscosity from MEMFCS for eGFP-CaM in both crowded dextran and dextran size mixtures (Table 4). If both parameters are allowed to vary (stretched-exponential fits of Eq. 2), then there is no clear trend in either, but when $n = 1$ (simple-exponential fits) is used, β is seen to depend on the polymer MW. A connection

between polymer phenomenology and polymer theory can be obtained through selection of an appropriate polymer model.

Polymer model comparison for single dextran sizes

There are two prominent polymer models that propose the functional dependence of n and β in polymer phenomenology, namely, the de Gennes-Langevin-Rondelez (GLR) model and the Phillies hydrodynamic model (39,40). These models appear to be mutually exclusive, because the GLR model predicts dependence of β on probe size but not on polymer MW, whereas the hydrodynamic model predicts a $\beta \approx \mathrm{MW}^{0.8}$ dependence but not a probe-size dependence. Although the GLR model appears to be valid for many polymers (36), it is not clear whether it applies for highly branched polymers, since probe mobility for Dex 500 and ficoll 70 were shown to be only mildly affected by probe size (35). It is important to note that both models were only valid for up to the semidilute regime, although the hydrodynamic model has recently been extended to the crowded regime (3). The GLR model predicts that the transition between the semidilute and crowded regimes is supposed to occur at the critical concentration, c^*, where the probe size reaches the correlation length of the polymer network and polymer ''entanglement'' ensues (39). The Phillies model predicts instead that no ''entanglement'' ensues, but rather that only hydrodynamics (but not hydrodynamic screening) is important. It is not expected that c^* will remain constant for different dextran sizes, and it has been estimated using dynamic light scattering that for Dex 40, $c^* = 21\%$ (w/v); for Dex 150, $c^* = 11\%$ (w/v) (14); and for Dex 500, $c^* < 1\%$ (w/v) (P. Vekilov, University of Houston, personal communication, 2008). No clear critical concentration was seen for any dextran size studied here, although the number of data points might be too few to show the subtle change from the semidilute to the crowded regime. At each crowding level, dextran is likely to have different levels of compression and hydration with slightly different size and shape, depending on its branching (11,16,41,42), and this would impact the values of n and β, since those parameters, obtained from a fit over all crowding levels, are indirectly dependent on excluded volume.

Applying the universal polymer equation to eGFP-CaM's major microviscosity, we found values of n between 0.70 and 1.135 for dextran sizes from 10 to 500 kDa, and of 1.105 for the Dex10:500 mixtures. However, simple exponential fits obtained by fixing n at 1 resulted in a better goodness of fit in all cases except for the 250-kDa dextran.

When both free parameters n and β are allowed to vary, there is no clear trend in either (Table 4), whereas when n is fixed ($n = 1$), a size-dependent trend appears in β (Fig. 6 *B*, *solid line*) that is best fit with a power law of $\sim\mathrm{MW}^{0.11}$ rather than the $\sim\mathrm{MW}^{0.8}$ power law suggested by the Phillies hydrodynamic model (3). However, the trend is irregular and also appears to have a low and a high value, with the transition near where the size of the viscogen becomes larger than the size of the probe. Ultimately, both models fail to fully describe the data, but results strongly indicate a preference for the hydrodynamic over the entangled viewpoint, and indicates the absence of hydrodynamic screening in agreement with the Phillies model since anomalous diffusion is not found. The dependence of β on probe size, predicted by the GLR model, was not tested in this study, although the GLR model assertion that there would be no polymer MW dependence was clearly refuted. The dextran MW dependence of β predicted by the Phillies model was confirmed, but the data did not fit the predicted functional form. It is likely that a new polymer model is needed that can incorporate both the probe and viscogen size dependence of β. Even without a perfect polymer model, polymer phenomenology still applies, and the experimental determination of n and β for a given probe/polymer system allows microviscosity to be predicted for any crowding level in the crowded regime.

Polymer phenomenology for dextran size mixtures

We find that the universal polymer equation can be applied to the major microviscosity for mixtures of different sizes of dextran as well as individual sizes. A simple exponential ($n = 1$) fit for Dex10:500 with a size intermediate β (Fig. 6 *B dashed line*) indicates that the probe experiences an ''average'' major microviscosity when surrounded by viscogen which has sizes smaller to, equal to and larger than its size. This interpretation is supported by the fact that the average fit of the universal polymer equation to the individual dextran size data over the entire concentration range (Fig. 6 *A*) yields a β in close agreement with the Dex10:500 mixture. This indicates that the major microviscosity of dextran mixtures can be understood as a type of ''average'' behavior of its component size composition. By experimentally determining n and β for any viscogen size composition, the probe's major microviscosity can be well described as a function of crowding level. This suggests that the crowding level is a more important factor than viscogen size for most of a probe's mobility in the presence of mobile obstacles.

Microviscosity versus bulk viscosity for cytosolic mimetic crowding level

We find that at 10% (w/v), both in dextran mixtures and in individual dextran sizes, the major component of microviscosity is constant (Fig. 4, *A* and *B*) and is slowed approximately threefold compared to that determined in buffer. This value is consistent with the viscosity calculated for diffusion in a cell's cytoplasm (1). This result supports the idea that crowding level, and not crowder size or mixture size composition, has the dominant effect on probe mobility. In Fig. 4, it can be seen from the major microviscosity that whether the mobile obstacles are the same size as the probe,

or larger or smaller, or even a mixture of sizes, most probe translational mobility is the same, as long as crowding density is constant among different solutions. The fraction of available volume excluded to the probe must be approximately constant for the different solutions at constant crowding density. This result is surprising based on volume exclusion expected from nonpenetrating hard spheres, and highlights the failure of this assumption for dextran. Because of the dominance of the major microviscosity, one could argue that the minor microviscosity should be ignored and a single-component model used instead. Probe diffusion in the mixtures strongly suggests that this is not the case and yields a physical interpretation for the two minor microviscosities detected. Minor microviscosity in the smaller-size mixture compositions (Dex10:25 and Dex10:40) corresponds to freely diffusing probe, and in the larger-size mixtures (Dex40:500 and Dex70:500) corresponds to probe experiencing microviscosity of equal magnitude to the bulk viscosity (Fig. 4 *A*).

The bulk viscosity can agree or diverge from the major microviscosity (Fig. 4), becausethe bulk viscosity, unlike the major microviscosity, is strongly influenced by dextran size and increases as a power law, $\sim MW^{0.6}$ (Fig. 4 *B*). It is reasonable that dextran's bulk viscosity in crowded solutions increases as a power law with dextran size because its intrinsic viscosity (nothing to do with β-power law) is known to increase by $\sim MW^{0.47}$ at a fixed dilute crowding level (18). A minor microviscosity was detected for eGFP-CaM in Dex 40, 150, and 250 at 10% (w/v) (Fig. 4 *B*). For our 43-kDa probe in 40 kDa dextran, this minor microviscosity is significantly larger than the bulk viscosity, indicating that when the probe and viscogen are of comparable size for this crowding level, this fraction of probe is somehow trapped and appears effectively immobile. A microviscosity slightly higher than the bulk viscosity could be explained by the fact that rheological measurements apply shear to the fluid, which stretches polymers out, resulting in a viscosity decrease, whereas in FCS there is no shear. This effect should be negligible in dextran, because it has Newtonian fluid properties, attributed to its branching, in which its bulk viscosity stays constant rather than decreasing with increased shear rate (18). By plotting microviscosity and bulk viscosity together (Fig. 4), one can clearly see the complicated deviations from the SE equation, in which multiple microviscosities exist that can have a component in agreement with the bulk viscosity and an additional component that is less than the bulk viscosity.

CONCLUSIONS

MEMFCS is a powerful alternative to the anomalous model for describing diffusion in solutions of mobile obstacles, offering increased resolution and possible physical interpretation of diffusive mechanisms. We applied MEMFCS to analyze eGFP-CaM (43 kDa) diffusion in dextran solutions of sizes ranging from 0.25 to 12 times that of the probe, and in mixtures of the different dextran sizes. Diffusive mechanisms from apparent nanostructuring of the environment were quantified in terms of single or multiple diffusive terms experienced by the probe. In general, the frequency of nanostructuring increases with dextran size and crowding level, and this nanostructuring was suppressed when dextrans of all sizes were combined. We find that the minor component of microviscosity, when detected, is usually either from a probe diffusing as in buffer, or from a probe diffusing at a rate consistent with bulk viscosity. In contrast, the major component of microviscosity increases with crowding level with a simple exponential, which agrees with polymer phenomenology. Its parameter β increases with dextran size, as predicted by the Phillies hydrodynamic model, but does not agree with the predicted functional form of $\sim MW^{0.8}$. We show that polymer phenomenology can also be extended to describe probe diffusion in crowded mixtures, which would be more representative of the intracellular milieu. The additional components captured by MEMFCS, which are discarded when using polymer models, indicate that there may be additional diffusion coefficients for the same probe within these crowded mixtures. These novel differences noted in probe mobility in crowded polymer solutions highlight the need for a comprehensive theory of microviscosity.

SUPPLEMENTARY MATERIAL

To view all of the supplemental files associated with this article, visit www.biophysj.org.

We thank Dr. Sudipta Maiti for kindly providing the MEMFCS software, and Drs. Matteo Pasquali and Peter Vekilov for providing instrumental rheometry support, dextran polymer insight, and fruitful discussions.

This work was supported by grants from the National Institutes of Health/National Institute of Neurological Disorders and Stroke (NS26086 and NS038310). A.B.G. acknowledges support through the Houston Area Molecular Biophysics Training program (T32 GM008280). H.S. acknowledges support from a training fellowship from the Keck Center Nanobiology Training Program of the Gulf Coast Consortia (National Institutes of Health grant 2 R90 DK071054-03S1).

REFERENCES

1. Luby-Phelps, K. 2000. Cytoarchitecture and physical properties of cytoplasm: volume, viscosity, diffusion, intracellular surface area. *Int. Rev. Cytol.* 192:189–221.
2. Konopka, M. C., I. A. Shkel, S. Cayley, M. T. Record, and J. C. Weisshaar. 2006. Crowding and confinement effects on protein diffusion in vivo. *J. Bacteriol.* 188:6115–6123.
3. Phillies, G. D. J. 2007. Optical Probe Diffusion in Polymer Solutions. arXiv:0705.3222v1 [cond-mat.soft].
4. Sanabria, H., Y. Kubota, and M. N. Waxham. 2007. Multiple diffusion mechanisms due to nanostructuring in crowded environments. *Biophys. J.* 92:313–322.
5. Dittrich, P., and P. Schwille. 2001. Photobleaching and stabilization of fluorophores used for single-molecule analysis with one- and two-photon excitation. *Appl. Phys. B.* 73:829–837.

6. Yamniuk, A. P., and H. J. Vogel. 2004. Calmodulin's flexibility allows for promiscuity in its interactions with target proteins and peptides. *Mol. Biotechnol.* 27:33–57.
7. Junge, H. J., J.-S. Rhee, O. Jahn, F. Varoqueaux, J. Spiess, M. N. Waxham, C. Rosenmund, and N. Brose. 2004. Calmodulin and Munc13 form a Ca^{2+} sensor/effector complex that controls short-term synaptic plasticity. *Cell.* 118:389–401.
8. Kim, S. A., K. G. Heinze, M. N. Waxham, and P. Schwille. 2004. Intracellular calmodulin availability accessed with two-photon cross-correlation. *Proc. Natl. Acad. Sci. USA.* 101:105–110.
9. Kim, S. A., K. G. Heinze, K. Bacia, M. N. Waxham, and P. Schwille. 2005. Two-photon cross-correlation analysis of intracellular reactions with variable stoichiometry. *Biophys. J.* 88:4319–4336.
10. Minton, A. P. 2006. How can biochemical reactions within cells differ from those in test tubes? *J. Cell Sci.* 119:2863–2869.
11. Venturoli, D., and B. Rippe. 2005. Ficoll and dextran vs. globular proteins as probes for testing glomerular permselectivity: effects of molecular size, shape, charge, and deformability. *Am. J. Physiol. Renal Physiol.* 288:F605–F613.
12. Kozer, N., Y. Y. Kuttner, G. Haran, and G. Schreiber. 2007. Protein-protein association in polymer solutions: from dilute to semidilute to concentrated. *Biophys. J.* 92:2139–2149.
13. Lavalette, D., M. A. Hink, M. Tourbez, C. Tetreau, and A. J. Visser. 2006. Proteins as micro viscosimeters: Brownian motion revisited. *Eur. Biophys. J.* 35:517–522.
14. Furukawa, R. A.-L. J. L., and B. R. Ware. 1991. Self-diffusion and probe diffusion in dilute and semidilute solutions of dextran. *Macromolecules.* 24:599–605.
15. Phillies, G. D. J., J. Gong, L. Li, A. Rau, K. Zhang, L. P. Yu, and J. Rollings. 1989. Macroparticle diffusion in dextran solutions. *J. Phys. Chem.* 93:6219–6223.
16. Bovey, F. A. 1959. Enzymatic polymerisation I: molecular weight and branching during the formation of dextran. *J. Polym. Sci.* [*B*]. 35:167–182.
17. Senti, F. R., N. N. Hellman, N. H. Ludwig, G. E. Babcock, R. Tobin, C. A. Glass, and B. L. Lamberts. 1955. Viscosity, sedimentation, and light-scattering properties of fraction of an acid-hydrolyzed dextran. *J. Polym. Sci. [B].* 17:527–546.
18. Carrasco, F., E. Chornet, and R. P. Overend. 1989. A generalized correlation for the viscosity of dextrans in aqueous solutions as a function of temperature, concentration, and molecular weight as low shear rRates. *J. Appl. Polym. Sci.* 37:2087–2098.
19. Maiti, S., U. Haupts, and W. W. Webb. 1997. Fluorescence correlation spectroscopy: diagnostics for sparse molecules. *Proc. Natl. Acad. Sci. USA.* 94:11753–11757.
20. Berland, K., and G. Shen. 2003. Excitation saturation in two-photon fluorescence correlation spectroscopy. *Appl. Opt.* 42:5566–5576.
21. Nagy, A., J. Wu, and K. M. Berland. 2005. Observation volumes and gamma-factors in two-photon fluorescence fluctuation spectroscopy. *Biophys. J.* 89:2077–2090.
22. Wu, J., and K. Berland. 2007. Fluorescence intensity is a poor predictor of saturation effects in two-photon microscopy: artifacts in fluorescence correlation spectroscopy. *Microsc. Res. Tech.* 70:682–686.
23. Mertz, J. 1998. Molecular photodynamics involved in multi-photon excitation fluorescence microscopy. *Eur. Phys. J. D.* 3:53–66.
24. Widengren, J., U. Mets, and R. Rigler. 2003. Flourescence correlation spectroscopy of triplet states in solution: a theoretical and experimental study. *J. Phys. Chem.* 99:13368–13379.
25. Periasamy, N., and A. S. Verkman. 1998. Analysis of fluorophore diffusion by continuous distributions of diffusion coefficients: application to photobleaching measurements of multicomponent and anomalous diffusion. *Biophys. J.* 75:557–567.
26. Langowski, J., and R. Bryan. 1991. Maximum entropy analysis of photon correlation spectroscopy data using a Bayesian estimate for the regularization parameter. *Macromolecules.* 24:6346–6348.
27. Skilling, J., and R. K. Bryan. 1984. Maximum entropy image reconstruction: general algorithm. *Mon. Not. R. Astron. Soc.* 211:111–124.
28. Bryan, R. K. 1990. Maximum entropy analysis of oversampled data problems. *Eur. Biophys. J.* 18:165–174.
29. Sengupta, P., K. Garai, J. Balaji, N. Periasamy, and S. Maiti. 2003. Measuring size distribution in highly heterogeneous systems with fluorescence correlation spectroscopy. *Biophys. J.* 84:1977–1984.
30. Iyer, V., M. J. Rossow, and M. N. Waxham. 2004. Focal volume characterization using multiphoton fluorescence correlation spectroscopy (MP-FCS). *Proc. SPIE.* 5323:146–159.
31. Dunn, A. K., V. P. Wallace, M. Coleno, M. W. Berns, and B. J. Tromberg. 2000. Influence of optical properties on two-photon fluorescence imaging in turbid samples. *Appl. Opt.* 39:1194–1201.
32. Schwille, P., J. Korlach, and W. W. Webb. 1999. Fluorescence correlation spectroscopy with single-molecule sensitivity on cell and model membranes. *Cytometry.* 36:176–182.
33. Banks, D. S., and C. Fradin. 2005. Anomalous diffusion of proteins due to molecular crowding. *Biophys. J.* 89:2960–2971.
34. Chirife, J., and M. P. Buera. 1997. A simple model of predicting the viscosity of sugar and oligosaccharide solutions. *J. Food Eng.* 33:221–226.
35. Dauty, E., and A. S. Verkman. 2004. Molecular crowding reduces to a similar extent the diffusion of small solutes and macromolecules: measurement by fluorescence correlation spectroscopy. *J. Mol. Recognit.* 17:441–447.
36. Michelman-Ribeiro, A., F. Horkay, R. Nossal, and H. Boukari. 2007. Probe diffusion in aqueous poly(vinyl alcohol) solutions studied by fluorescence correlation spectroscopy. *Biomacromolecules.* 8:1595–1600.
37. Masaro, L., and X. X. Zhu. 1999. Physical models of diffusion for polymer solutions, gels and solids. *Prog. Polym. Sci.* 24:731–775.
38. Phillies, G. D. J., and D. Clomenil. 1993. Probe diffusion in polymer solutions under theta and good conditions. *Macromolecules.* 26:167–170.
39. Langevin, D., and F. Rondelez. 1978. Sedimentation of large colloidal particles through semidilute polymer solutions. *Polymer.* 19:875–882.
40. Phillies, G. D. J. 1998. Derivation of the universal scaling equation of the hydrodynamic scaling model via renormalization group analysis. *Macromolecules.* 31:2317–2327.
41. Granath, K. A. 1958. Solution properties of branched dextrans. *J. Colloid Sci.* 13:308–328.
42. Ogston, A. G., and B. N. Preston. 1979. The molecular compression of dextran. *Biochem. J.* 183:1–9.